PAPER

Comparative study of the strongest solid Lewis acids known: ACF and *HS*-AlF₃†‡

Beatriz Calvo,§[a] Clara Patricia Marshall,§[a,b] Thoralf Krahl,[a,c] Jutta Kröhnert,[d] Annette Trunschke, [ID] [d] Gudrun Scholz,[a] Thomas Braun [ID] *[a] and Erhard Kemnitz [ID] *[a,c]

Aluminium chlorofluoride (ACF) and high-surface aluminium fluoride (*HS*-AlF₃) were analyzed by a set of characterization methods to assess their acidic properties: NH₃-TPD, CO adsorption followed by DRIFTS, CD₃CN-PAS-FTIR and MAS NMR spectroscopy after ¹⁵N-pyridine adsorption. Both catalysts contain very strong and medium-strong Lewis acid sites as confirmed by CO adsorption, in which small differences arise from the morphological properties of each catalyst, with ACF being microporous and *HS*-AlF₃ meso-porous. Shifts of the CO vibration band of up to 77 cm⁻¹ were observed, which account for very strong Lewis acid sites. In addition, very strong Lewis acid sites could be identified by CD₃CN-PAS for both catalysts, exhibiting a shift of 95 cm⁻¹ from free nitrile, the highest ever reported for a solid Lewis acid.

Introduction

Understanding the composition and properties of heterogeneous catalysts is one of the major challenges in the field, since reactivity itself does not give direct information about how a reaction proceeds on the catalyst active sites. Acid catalysts, either Lewis and/or Brønsted acidic, pose an even more complex challenge for the quantification and the identification of their reactive sites, and research has focused on several methods to achieve this goal, involving *in situ* characterization methods and spectroscopic studies after adsorption of probe molecules.[1–6]

Diverse characterization methods have different limitations and advantages, but the use of only one of them does not permit a full understanding of the catalytic system. Therefore, a research approach where an array of techniques are used to characterize a material allows a better insight *via* a complementary way. Adsorption of probe molecules combined with a spectroscopic characterization is a standard approach for characterization of heterogeneous catalysts; in particular for

solid acid catalysts; basic probe molecules such as pyridine, CO or acetonitrile are commonly used.[2,5] In this regard, carbon monoxide is very useful since it combines weak σ-donor and strong π-base characteristics, leading to the formation of synergetic interaction in M–CO bonds at a large number of metal centers. Based on this bonding, a decreasing CO frequency in the IR spectra of transition element complexes is an accepted measure of increasing negative charge buildup on the metal center.[7] Alternatively, if the M–CO interaction does not involve d-electrons, the CO stretching frequency shifts to higher wavenumbers. This behavior is the result of the Stark effect associated with the positive electric field of the adsorptive cation, and the ν(CO) shift is proportional to the strength of the electric field sensed by CO, providing, therefore, a tool for the characterization of the Lewis acidity in solid materials.[8–10] Solid-state NMR spectroscopy is an alternative useful tool for the study of active sites in heterogeneous catalysts. This technique uses also probe molecules such as pyridine, phosphines or trialkylphosphine oxides, which interact with the Lewis and Brønsted sites of the solid material providing information which complements that obtained by vibrational spectroscopy.[11–15]

ACF and *HS*-AlF₃ are very strong Lewis acids, equal or even stronger than SbF₅ in some cases. Well-known synthesis procedures make these materials available as heterogeneous catalysts for a large variety of reactions.[16–19] Although these AlF₃-based catalysts have many essential properties in common, they exhibit small differences to some extent. The main distinction between ACF and *HS*-AlF₃ arises from their very starting point as catalysts: their synthesis procedure. It may seem trivial at first glance, but it is not, since it determines their

[a]Department of Chemistry, Humboldt-Universität zu Berlin, Brook-Taylor-Straße 2, D-12489 Berlin, Germany. E-mail: erhard.kemnitz@chemie.hu-berlin.de, thomas.braun@cms.hu-berlin.de
[b]School of Analytical Sciences Adlershof (SALSA), Humboldt-Universität zu Berlin, Unter den Linden 6, D-10099 Berlin, Germany
[c]Nanofluor GmbH, Rudower Chaussee 29, D-12489 Berlin, Germany
[d]Department of Inorganic Chemistry, Fritz-Haber-Institute der Max-Planck-Gesellschaft, Faradayweg 4-6, D-14195 Berlin, Germany

porosity and thus sorption properties. ACF is synthesized by a very exothermic Cl/F exchange reaction, starting from $AlCl_3$ as a precursor suspended in CCl_4. Aluminium chloride is by itself a powdery substance, and as ACF is produced from it, as described by Krespan et al., it is a "finely divided powder, even when aluminum chloride of larger particle size is used as the starting material".[17] This is in contrast to the two-step preparation of HS-AlF_3, which consists of a fluorolytic sol–gel reaction starting from aluminium isopropoxide followed by an activation step under flow of a fluorinating gas.[18] The isopropoxide groups in the HS-AlF_3 precursor create spatial distortion, creating mesopores as these groups are fully transformed to Al–F bonds in the activation step. The final catalyst is a granular powder, in contrast to the fine powder of ACF. For both catalysts, several studies have analyzed the effect that small changes in the synthesis parameters produce: interestingly, ACF always remained microporous, and HS-AlF_3 exclusively mesoporous.[20,21]

Beside many common properties, both phases exhibit strong different properties regarding thermal and hydrolysis stability. Based on extremely strong Lewis acid surface sites which origin from coordinatively undercoordinated Al-surface sites (cus), both phases strongly bind water molecules. In the case of HS-AlF_3, this process is reversible, that is, adsorbed water can be completely removed under careful heating in a nitrogen flow, and thus totally recover the former high Lewis acidity. In contrast, ACF undergoes very rapidly complete hydrolysis of the Al–Cl bonds in a few seconds of contact to ambient atmosphere, which makes the recovery of the high Lewis acidity impossible. Thus, ACF only can be used when generated under *in situ* conditions or under strictly inert conditions. Whereas HS-AlF_3 is stable even above 700 °C, ACF undergoes irreversible decomposition into crystalline AlF_3 and $AlCl_3$ between 400 and 450 °C depending on the chemical nature of the surrounding gas atmosphere.

It is interesting to compare also both catalysts regarding their reactivity, since they also show some similarities and some differences. For that purpose, three reactions already reported, namely the isomerization of 1,2-dibromohexafluoropropane,[16,18] the hydroarylation of ethene[22] and the dehydrochlorination of chlorinated toluenes[23] (see Fig. 1) can be chosen as examples. The activation of carbon–halogen bonds occurring in the isomerization of 1,2-dibromohexafluoropropane demands extremely strong Lewis acid sites, the strong Lewis acid $AlCl_3$ needs a temperature of 150 °C to achieve 74% conversion and even SbF_5, considered as one of the strongest known Lewis acids,[24] needs *ca.* 80 °C to achieve conversion >90%.[25] In contrast, in the case of ACF and HS-AlF_3, this reaction occurs at room temperature, and after only 2 hours full conversion is achieved. Another interesting reaction to compare is the hydroarylation of ethene. After only 5 minutes at room temperature full conversion is observed for ACF, however, HS-AlF_3 exhibits lower reactivity under the same experimental conditions.[22] Dehydrochlorination reactions for both catalysts also showed that sterically demanding substrates, *e.g.* dichlorotoluene (Fig. 1 and 2), need lower temperature and time to react in presence of HS-AlF_3 as compared to ACF.[23]
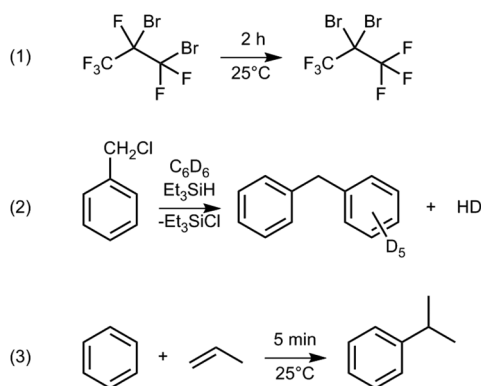

Fig. 1 Reported reactions for ACF and HS-AlF_3: isomerization of carbon halogen bonds (1), dehydrochlorination (2) and hydroarylation (3).
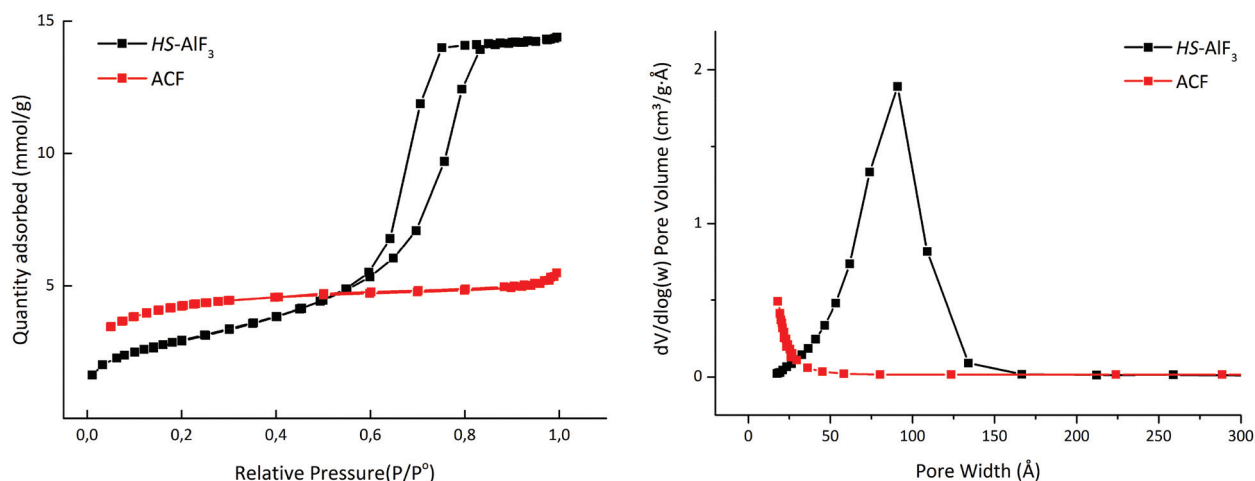

Fig. 2 N_2 adsorption/desorption isotherms at −196 °C (left) and pore size distribution according to the BJH model (right) for ACF and HS-AlF_3.

Although both very strong solid acids have been intensively characterized and catalytically investigated over the past years, a detailed characterization of the surface acid sites of ACF is still lacking because – in contrast to HS-AlF$_3$ which is hydrolysis resistant – it undergoes complete hydrolysis in a few seconds of contact with ambient atmosphere. Thus, for HS-AlF$_3$ a comprehensive characterization of acidic surface sites by CO-adsorption followed by FTIR spectroscopy has been reported, all attempts to do the same for ACF failed at that time. Thus, so far HS-AlF$_3$ is, to the best of our knowledge, the only solid exhibiting CO adsorption bands as high as 2220 cm^{-1}, suggesting the presence of extremely strong Lewis acid sites.[26] On the other side, there are many catalytic reactions for which ACF shows equal high or even slightly higher catalytic activity than HS-AlF$_3$.[19]

Herein, we report a combination of attempts to analyze the surface of ACF and HS-AlF$_3$. This includes studies on CO adsorption by diffuse reflectance infrared Fourier transform spectroscopy (DRIFTS), MAS NMR spectroscopy investigations with ^{15}N-pyridine as a probe molecule, as well as NH$_3$-TPD experiments, CD$_3$CN-photoacoustic IR spectroscopy, and specific BET surface area measurements. In order to compare these two strongest known solid Lewis acids, HS-AlF$_3$ and ACF, the data were obtained under the same conditions to provide a systematic and comprehensive study of their characteristics. The results have implications for the mechanisms of catalytic conversions by these materials, which are capable of activating C–H and C–F bonds.[22,23,27–29]

Experimental section

General procedures

ACF and HS-AlF$_3$ were synthesized according to methods published in the literature.[18,30,31] All manipulations were carried out under Ar atmosphere using standard Schlenk techniques. For the samples loaded with ^{15}N labelled pyridine (Sigma Aldrich, water by Karl Fischer 0.5%), 1 g of the catalyst was treated with an excess (40 µl, 1 mmol) and the mixture was stirred for 1 h at 150 °C, then evacuated for 17 h at 70 °C.

NH$_3$-TPD

The samples (about 0.2 g) were first heated under nitrogen up to 300 °C, and then exposed at 120 °C to NH$_3$. After flushing the excess of NH$_3$ at 120 °C with N$_2$ for 1 h and cooling to 80 °C, the TPD program was started (10 °C min^{-1} up to 500 °C, keeping for 30 min at 500 °C). Desorbed NH$_3$ was monitored continuously *via* IR spectroscopy (FT-IR System 2000, PerkinElmer), and quantified by back-titration with sodium hydroxide solution, to determine the total amount of acid sites.

CD$_3$CN-FTIR-PAS

Lewis acid sites on ACF and HS-AlF$_3$ were studied with FTIR photoacoustic spectroscopy after CD$_3$CN adsorption. Deuterated acetonitrile was adsorbed on the sample at 150 °C, and the FTIR spectra of acetonitrile-loaded samples were

recorded between 4000 and 400 cm^{-1} using a MTEC 200 photoacoustic cell and a FTIR system 2000 PerkinElmer instrument.

Elemental analysis

An EURO EA device (HEKATech GmbH) was used to determine the amount of hydrogen, carbon and nitrogen from the samples.

Surface area determination

The surface area of the samples were determined using nitrogen adsorption by means of a Micromeritics ASAP 2020 instrument. Before each measurement, the samples were degassed at 5×10^{-5} mbar for 12 h at 200 °C. The isotherms were analyzed employing the Brunauer–Emmett–Teller (BET) model for surface area and Barrett–Joyner–Halenda (BJH) for pore size and volume. For an estimation of the microporosity, t-plots were used to model the isotherms using the calculations provided by the program ASAP2020, based on the Harkins and Jura thickness estimation.[32]

MAS NMR spectroscopy

All solid-state NMR experiments were performed on a Bruker AVANCE 400 spectrometer. ^{19}F and ^{27}Al NMR spectra were recorded (Larmor frequencies: ν(^{19}F) = 376.4 MHz; ν([27]Al) = 104.3 MHz) using a 2.5 mm MAS probe (Bruker Biospin). All spectra were recorded at a spinning frequency of ν_{rot} = 20 kHz or 25 kHz. ^{19}F MAS NMR (I = 1/2) spectra were recorded with a π/2 pulse duration of p1 = 3.6 µs, a spectrum width of 400 kHz, and a recycle delay of 5 s. Existent background signals were suppressed with the application of a phase-cycled depth pulse sequence according to Cory and Ritchey.[33] The rotor-synchronized ^{19}F NMR spin-echo experiments were registered with a recycle delay of 5 s, an accumulation number of 1024 and a dipolar evolution time of 0.25 ms. ^{1}H–^{15}N CP-MAS NMR (cross-polarization magic angle sample spinning) experiments were carried out in a 7 mm rotor using a [1]H 90° pulse length of 6.5 µs, a contact time of 3 ms, and a recycle delay of 5 s. Up to 14 336 scans were accumulated, and high power proton decoupling (TPPM) was applied. Quantitative reconstruction of the central lines of the ^{1}H and ^{1}H–^{15}N CP-MAS NMR spectra were performed using the DMFIT software. All isotropic chemical shift values are referenced against zero of the IUPAC standards using [15]ND$_4$Cl (^{15}N), α-AlF$_3$ (^{19}F, [27]Al) and adamantan (^{1}H) as secondary standards for the measurements.

CO adsorption followed by DRIFTS

In situ DRIFTS measurements were conducted using an Agilent Cary 680 FTIR spectrometer equipped with an MCT detector at a spectral resolution of 2 cm^{-1} and an accumulation of 512 scans. The sample cup of an *in situ* cell (Harrick Praying Mantis™ diffuse reflectance attachment DRP-DF8 in combination with a low-temperature reaction chamber CHC-CHA-3) was filled with ~100 mg of the catalyst in a glovebox. The cell was closed in the glovebox, locked out and afterwards DRIFT spectra of sequential dosing of CO (0.124–162 mbar equili-

brium pressure) were collected at −196 °C. To avoid moisture contact, the cell was previously heated at 350 °C for 15 minutes and kept under dynamic vacuum for 48 h in the glovebox. A spectrum of KBr under dynamic vacuum at −196 °C served as background for the measurements.

Results

Surface area determination

When studying heterogeneous catalysts, their morphological properties are important aspects, *e.g.* pore size and pore volume, and specific surface area. Both catalysts ACF and *HS*-AlF$_3$ have already been investigated by means of nitrogen sorption,[18,34] but for our purposes, we repeated even these measurements in order to have a consistent set of data generated under the same conditions. In particular, we applied the empirical model of Lippens and de Boer to generate *t*-plots, and from these we estimated the micropore area of both catalysts.[35] There are other methods and models, which are more accurate to determine microporosity.[36] However, in this work just a rough estimation of the contribution of micropores and mesopores for each catalyst was of interest. The simplification of the *t*-plot as a model, using a standard multilayer thickness curve, needs to be taken into account. Table 1 exhibits the results for ACF and *HS*-AlF$_3$ as measured in this work. The corresponding isotherms are presented in Fig. 2 along with their pore size distributions according to BJH model.

Several points can be highlighted. *HS*-AlF$_3$ shows a type IV isotherm according to IUPAC and a characteristic hysteresis at $P/P_0 = 0.60$–0.80 associated with capillary condensation, typical of mesoporous materials. ACF, on the other hand, exhibits a type I isotherm. As an interesting fact, *HS*-AlF$_3$ has five times bigger pore volume as compared to ACF (0.50 *vs.* 0.11 cm^3 g^{-1}). The pore size distribution, following the BJH model, shows that *HS*-AlF$_3$ has mostly pores of a size between 50 and 150 Å, in the mesopore region. ACF on the other hand, has such small pores, that it exceeds the measuring limits of the equipment used. Between 15 (experimental limit in our conditions) and 50 Å, a tendency for smaller pores can be observed, but no real assumption can be drawn concerning the real pore size distribution in ACF. The IUPAC technical report recommends that values from BET model for solids with isotherm type I must not be treated as realistic accessible surface areas.[37] They

represent an apparent value, and this distinction needs to be considered when comparing microporous and mesoporous materials with the same BET model. Thus, a quantitative comparison of the surface areas by BET of ACF and *HS*-AlF$_3$ is not fully accurate from a methodological point of view. However, with a certain uncertainty, the measured value of ACF can be used for a rough comparison of the surface areas. Based on these experimental data, both catalysts possess similar surface areas. Based on *t*-plots analysis (Table 1, Fig. S6‡) modeling the micropore area, a rough comparison shows that most of the surface area by BET for ACF consists of micropore area, whereas for *HS*-AlF$_3$ the contribution is clearly lower (318 to 334 m^2 g^{-1} in ACF and 13 to 240 m^2 g^{-1} in *HS*-AlF$_3$). Undoubtedly, the main difference between both catalysts is related to the different physisorption properties. In the following sections, the role such properties play in the interpretation of catalytic reactivity as well as in acid-site characterization techniques will be discussed.

NH$_3$-TPD

This characterization technique provides information about the strength distribution of acid sites on solid surfaces and the total amount of acid sites, by quantification of the desorbed ammonia. Unfortunately, since ammonia interacts with both, Lewis and Brønsted acid sites, a distinction between both acid types is impossible. However, it provides a good imagination about the distribution of acid surface sites of different strength.

Fig. 3 shows the NH$_3$-TPD profiles for ACF and *HS*-AlF$_3$. In both materials, there is an offset at *ca.* 150 °C, reaching a maximum at *ca.* 210 °C. In this temperature interval, desorption of ammonia is almost two-fold higher for *HS*-AlF$_3$ than for ACF. Interestingly, the desorption for ACF is more pronounced than for *HS*-AlF$_3$, giving a minimum at *ca.* 160 °C. The less structured desorption profile for *HS*-AlF$_3$ in the temperature range 150 °C to *ca.* 260 °C is probably due to the higher surface loading with NH$_3$ but even here an accelerated release in the same interval from 210 to 260 °C can be observed. Both aluminium fluoride phases have in common a very strong desorption interval starting at around 300 °C reaching a

Table 1 Surface area and pore size for ACF and *HS*-AlF$_3$ as measured in this work

Catalyst	Surface area by BET [m^2 g^{-1}]	Pore size[a] [Å]	Pore volume [cm^3 g^{-1}]	*t*-Plot micropore area [m^2 g^{-1}]
ACF	334	<15	0.11	318
HS-AlF$_3$	240	90	0.50	13

[a] Determined from the pore size distribution according to the BJH model.
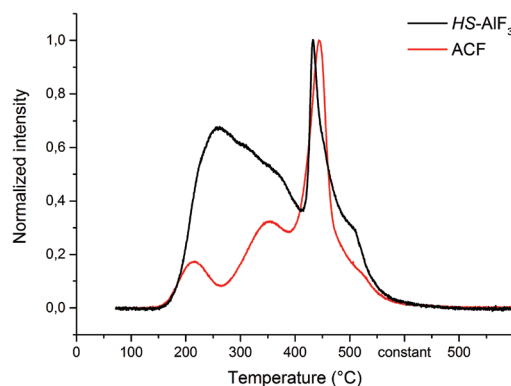
Fig. 3 NH$_3$-TPD profile for ACF (red) and *HS*-AlF$_3$ (black).

Table 2 Number of acid sites for ACF and *HS*-AlF$_3$ as determined by NH$_3$ TPD

Catalyst	Acid sites [μmol g^{-1}]	Density of acid sites [μmol m^{-2}]	% of medium-strength acid sites – before 400 °C[a]	% of very strong acid sites – after 400 °C[a]
ACF	1325	8.95	41.8	58.2
HS-AlF$_3$	1510	6.29	64.5	35.4

[a] Percentages calculated from integration of the TPD profiles.

maximum at *ca*. 350 °C and finally approaching the base line at around 450 °C. The number of total acid sites is comparable in both solids (see Table 2), but normalizing the density of acid sites over the surface area, ACF possesses a higher normalized value than *HS*-AlF$_3$, because its specific surface area is lower.

By estimating the relative contribution of the medium-strength and very strong acid sites, it can be observed that there is an inverse ratio when the catalysts are compared (see Table 2). ACF has slightly more of the very strong acid sites, whereas *HS*-AlF$_3$ has slightly more medium-strong acid sites. This comparison has to be taken with care, since ACF undergoes structural decomposition between 400 and 450 °C, depending on the atmospheric conditions.[38] Therefore, all the ammonia still adsorbed at surface sites is abruptly released when decomposition occurs, resulting in a very pronounced desorption peak. *HS*-AlF$_3$, on the other hand, is stable even above 500 °C, so it may be that the total amount of adsorbed ammonia is not fully desorbed at 500 °C were all these measurements were stopped due to technical limitation.

CD$_3$CN-FTIR-PAS

Acetonitrile is an interesting probe molecule for Lewis acid sites, being a soft base and less sterically crowded as other bases, like pyridine for example. The lone pair of electrons on

the nitrogen of acetonitrile can coordinatively bind to acid sites, thus modifying the properties of the C≡N bond and shifting the correspondent mode to wavenumbers of higher frequencies. Adsorbed nitriles on solid acid surfaces show a shift of around 10 cm^{-1} compared to their free gaseous mode, but it can even be higher, depending on the strength of the Lewis acid sites of the solid. Depending on the cationic centre, its ionization potential and radius, the position of the band of C≡N vibration can be shifted.[39] The stronger the Lewis acid sites are, the higher the shift will be.[2,5,40] A slight remark needs to be taken into account: our studies were performed with deuterated acetonitrile, in order to avoid Fermi resonance effects, which make the spectra and assignment of bands more complex. Therefore, comparison with other results, where non-deuterated acetonitrile was used, needs to be done with great care.[41] Several studies have been carried out on different oxides, zeolites and in particular for ACF, but so far not for *HS*-AlF$_3$.[5,34,42,43]

Fig. 4 displays the spectra obtained for both catalysts at different scan velocities (2.5 kHz and 5 kHz). Two spectra were measured: at a lower frequency, the signal-to-noise is improved and at a higher frequency, on the other hand, the resolution is improved. The position of the bands remains unchanged although slight differences in intensities appear. In the case of ACF, the spectrum shows three bands at 2363, 2337 and 2270 cm^{-1}, corresponding to the interaction of CN vibration to the different Lewis acid centers, compatible with published data.[34] The band at 2363 cm^{-1} had not been observed before: this could be due to some differences in sample handling or the synthesis procedure. Similarly, *HS*-AlF$_3$ loaded with adsorbed CD$_3$CN, exhibits three bands at 2363, 2331 and 2280 cm^{-1} of different intensity. Both spectra show different CN vibration bands corresponding to adsorbed nitrile molecules, blue shifted by *ca*. 69 cm^{-1} and 95 cm^{-1} compared to the free nitrile (2268 cm^{-1}). Large blue shifts correspond to interactions of the nitrile molecules with strong Lewis acid
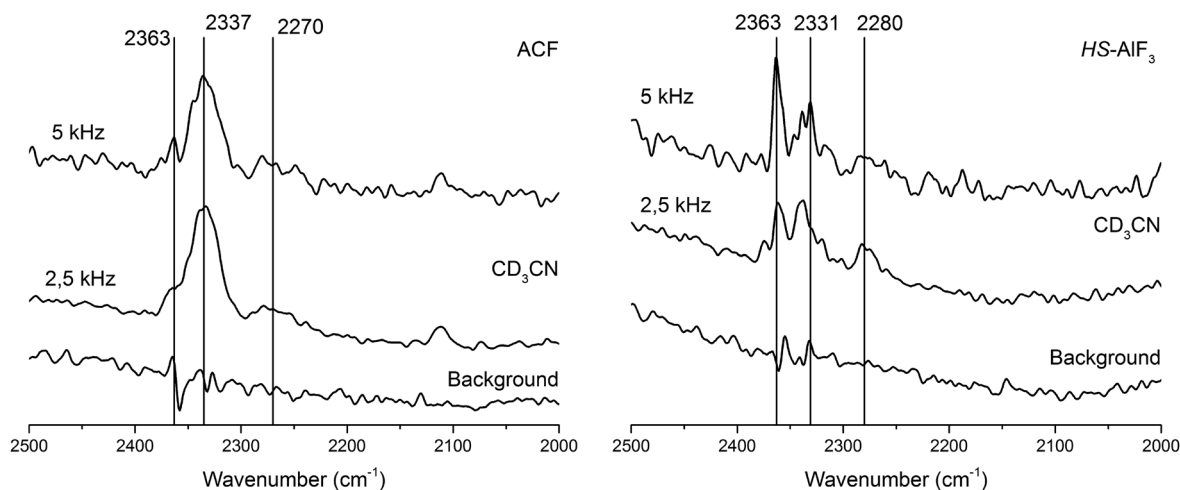
Fig. 4 CD$_3$CN FTIR-PAS for ACF (left) and *HS*-AlF$_3$ (right) at 2.5 kHz and 5 kHz. "Background" spectra refers to the FTIR-PA spectra for each catalyst without probe molecule.

centers. In the literature it is reported that well-known Lewis acidic solids, including γ-Al_2O_3, exhibit blue shifts between 57 and 47 cm^{-1}.[43,44] The values found for ACF and *HS*-AlF_3 are significantly higher than those, thus evidencing the very strong Lewis acidity of these two catalysts: this observed shift of 95 cm^{-1} is the highest ever reported, placing these AlF_3-based catalysts at the upmost top of the whole range of solid super Lewis acid catalysts.[34]

In the experimental set-up used herein, after adsorption of CD_3CN, the samples need to be transferred to the photoacoustic cell, suffering less than 30 seconds of air contact. Therefore, some of the very strong Lewis acid sites could be transformed into Brønsted in this procedure. It is reported in the literature that acetonitrile can also form weak complexes with Brønsted acid sites by hydrogen bonding, or it can be even protonated if such sites are strong enough. The position of such bands can be allocated in the range of 2290–2320 cm^{-1}, as from comparing several published results.[40,42,45,46] No definite value can be given, since each compound exhibits a unique shift, due to their chemical composition (different metal oxides, zeolites, *etc.*). When analyzing the spectra of CD_3CN adsorbed at ACF and *HS*-AlF_3, a problem arises, since the signal corresponding to proton-binding species to CD_3CN lies directly underneath that one of CD_3CN coordinatively bound to Al^{3+} Lewis acid sites. In other words, the presence of Brønsted acid sites in the catalysts can neither be confirmed nor excluded, since this technique does not allow to fully identify them.

CO adsorption monitored by DRIFTS

IR experiments using CO as probe molecule were performed because they allow not only to determine the presence of Lewis acid sites but also their relative strength. Brønsted acid sites can also be identified in some cases since the CO molecule is able to form a hydrogen-bond complex with such sites, which can be observed in IR spectroscopy. Several studies have been reported on various zeolites considering both Lewis and Brønsted acid sites, which recent reviews have addressed.[3,4] Table 3 summarizes the different IR signals that result from adsorbed CO species on different strength and type of acid sites at the solids. In the present case, it is important to keep

in mind that the phenomenon observed is based on electrostatic interactions between the Al^{3+} surface sites of the solid and the probe CO molecule since no transition metal is present. In a previous study,[26] one of us reported on the CO adsorption at *HS*-AlF_3 which had been activated in vacuum followed by heating and subsequent addition of CHF_3 *in situ*: this treatment eliminates possibly adsorbed water and ensures availability of a roughly clean, pure aluminium fluoride surface. This pre-treatment of samples is necessary because these extremely high Lewis-acidic AlF_3-phases attract very fast water from moist atmosphere. In contrast to *HS*-AlF_3, ACF becomes irreversibly hydrolyzed already after a few seconds contact with ambient atmosphere. Therefore, CO adsorption at ACF failed in our previous investigations, and was never studied. To better understand similarities and differences between these both very strong solid Lewis acids, CO adsorption experiments were therefore designed that allow the investigation of ACF under conditions that are described in detail in the experimental part. In order to allow a comparison of both AlF_3-phases, *HS*-AlF_3 was re-investigated in this work under the same conditions. Thus, DRIFTS experiments were carried out at −196 °C, after several steps of CO adsorption, until saturation was reached. DRIFTS is a powerful analytical tool for measuring the effect of CO adsorption on several materials, but it is important to keep in mind that relative differences can only be discussed in a qualitative fashion.

The spectrum obtained at each pressure for each catalyst was recorded, and afterwards an integral was calculated for the area between 2250 cm^{-1} and 2050 cm^{-1}. In Fig. 6, the results of these integrals *versus* CO pressure for both catalysts are presented. Both curves can be taken as CO adsorption isotherms. It is obvious that adsorption of CO on *HS*-AlF_3 is significantly more pronounced than on ACF over the measured partial pressure interval. Note that higher CO partial pressures are not shown due to the predominance of gas-phase CO in the spectra that interferes the integration. Fig. 5 shows the spectra at −196 °C of CO adsorption at ACF and *HS*-AlF_3 after consecutive exposure with CO doses. Expectedly, both samples show similar characteristics and also some differences. ACF and *HS*-AlF_3 contain very strong Lewis acid sites at 2226 cm^{-1} and 2220 cm^{-1}, respectively, as well as medium-strong Lewis acid sites at ≈2170–80 cm^{-1}. The very weak feature at ≈2131 cm^{-1} corresponds to physically adsorbed CO. This signal is close to free gaseous CO, which exhibits a stretching vibration at 2143 cm^{-1} (see Table 3). The position of these bands is in good agreement with those that were measured for *HS*-AlF_3 in our previous report.[26] Interestingly enough, both AlF_3-phases obviously are characterized by comparable very strong Lewis surface sites (at ≈2225 cm^{-1}) which – to the best of our knowledge – have never been reported for any other solid phase. However, differences obviously exist in the ratio of very strong to medium-strong Lewis acid sites. The experimental data imply a higher relative part of very strong sites in ACF when compared with *HS*-AlF_3. Considering the significantly higher CO coverage in case of *HS*-AlF_3 (*cf.* Fig. 6) it is obvious that after a dominant CO adsorption at the strongest sites, at a

Table 3 Wavenumbers of the ν(CO) stretching vibration of the samples and different adsorbed CO species

| Sample	CO stretching bands (cm^{-1})	Ref.
ACF	2226, 2174	This work
HS-AlF_3	2220, 2179	This work
HS-AlF_3	2240, 2225	25
Gaseous CO	2143	25
Physisorbed CO	2140–2150	25
CO at Brønsted acidic centers	2150–2180	25
CO at weak Lewis acidic centers	2160–2180	25
CO at medium Lewis acidic centers	2180–2200	25
CO strong Lewis acidic centers	2200–2220	25
CO at very Lewis acidic centers	>2220	25
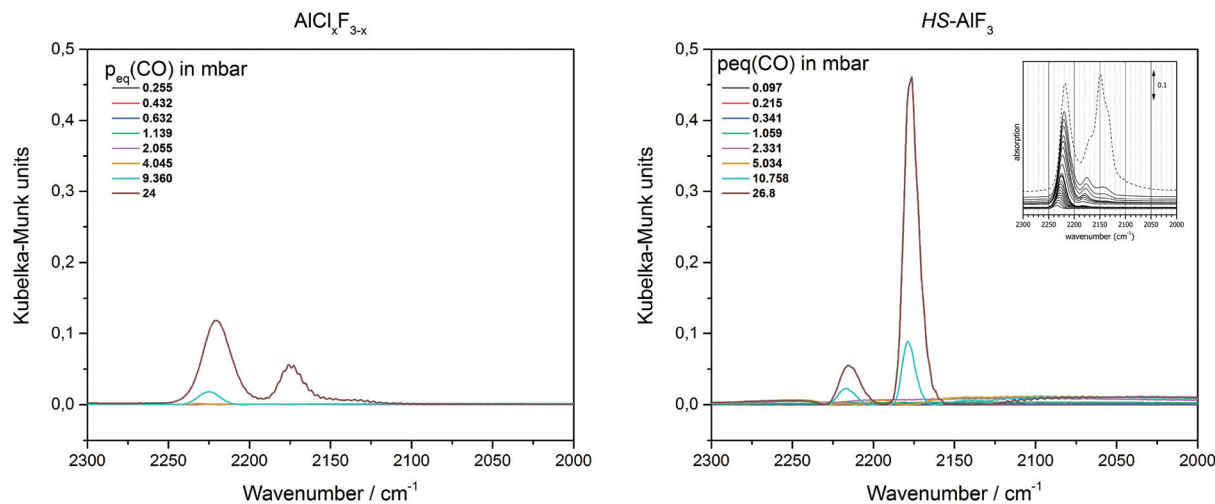
Fig. 5 CO adsorption for ACF (left) and *HS*-AlF₃ (right). The insert on the right corresponds to the already published data for *HS*-AlF₃, as reported by Krahl *et al.*[26]
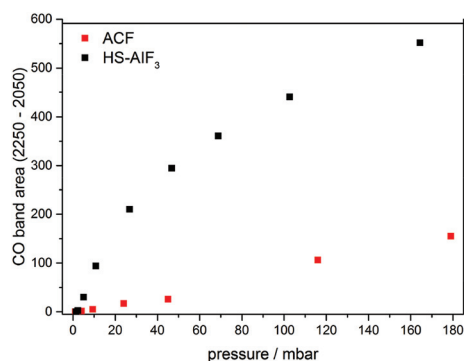

Fig. 6 Area of the bands of CO adsorption *vs.* pressure, for ACF (red) and *HS*-AlF₃ (black).

Fig. 7 ^{15}N solid state NMR chemical shift scale of various pyridine binding environments.

higher loading still available weaker surface sites will be covered by CO. To better illustrate this effect, the inset in Fig. 5 (right) is presented which displays the CO adsorption results reported previously for *HS*-AlF₃ in ref. 26. From this, it can be seen that at lower loadings with CO the distribution between very strong (≈ 2225 cm^{-1}) and medium-strong (≈ 2173 cm^{-1}) surface sites in *HS*-AlF and ACF is very similar when the loading is small enough. Thus, differences in the ratios of the bands at ≈ 2225 cm^{-1} and ≈ 2175 cm^{-1} between both phases as obtained herein are most probably due to different stages of the relative surface coverage.

MAS NMR spectroscopy

In recent years, it has been demonstrated that solid-state ^{15}N NMR spectroscopy is a reliable method for the quantification of Lewis and Brønsted acid centers.[11,47] The adsorption of ^{15}N-pyridine onto the matrix of a solid material such as, for example, ACF and *HS*-AlF₃ will form adducts that feature specific ^{15}N isotropic chemical shifts (δ_{iso}). The ^{15}N δ_{iso} of pyridine and pyridinium adsorbed at aluminium chlorofluoride
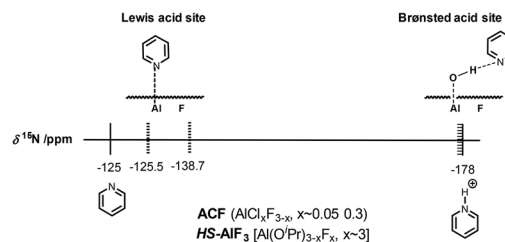
are -125 ppm and -178 ppm, respectively, typical chemical shift regions that can be used for the assessment of specific pyridine adducts that can be used for the characterization and quantification of Lewis *versus* Brønsted acid centers (Fig. 7).

Fig. 8 shows the ^{1}H MAS NMR spectra of pure ACF and *HS*-AlF₃ (black traces) and the spectra of the solids treated with ^{15}N-pyridine (blue traces). The latter spectra show distinct signals at $+14.1$ and $+15.9$ ppm that can be assigned to the pyridinium proton at ACF and *HS*-AlF₃, respectively. In the case of *HS*-AlF₃, the spectrum of the pure sample (black trace on the right) shows some residual signals that correspond to organic material arising from the preparation of the solid. The ^{1}H MAS NMR data demonstrate that the adsorption of ^{15}N-pyridine onto the amorphous matrices of ACF and *HS*-AlF₃ affords protonated pyridine molecules, implying the presence of Brønsted acid sites in these materials. Of course, some of these Brønsted centers could have been generated during the treatment with ^{15}N-pyridine, which, although highly pure, is not absolutely water free (0.099 ppm of water). The CO adsorption experiments shown on the previous section do not give any indication for these Brønsted acid sites, which should appear as a band at 2150 cm^{-1} originating from the bonding of CO to an OH moiety in the solid. Thus, we can assume that probably the small amount of water adsorbed during sample treatment
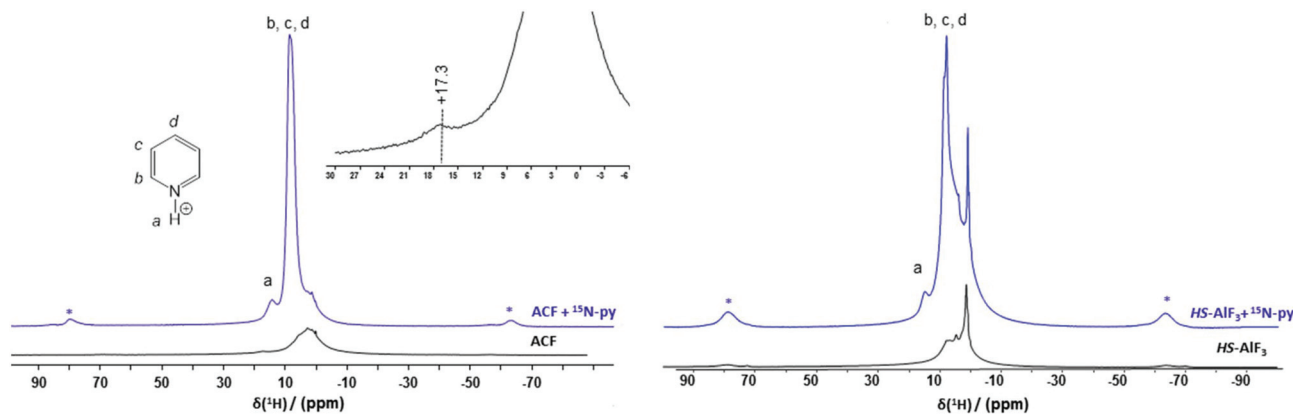
Fig. 8 ^{1}H MAS NMR spectra of ACF (left) and *HS*-AlF$_3$ (right) at 20 kHz rotation frequency: the black spectra correspond to the pure samples; the blue spectra correspond to the materials treated with ^{15}N-pyridine. Asterisks (*) mark spinning sidebands. Note: the black spectrum on the left hand side corresponds to the zoom spectrum of pure ACF.

Table 4 Elemental analysis of pure ACF and *HS*-AlF$_3$ together with the ^{15}N-pyridine adsorbed materials

| Sample	% C	% H	% N	% Py adsorbed calculated
ACF	0.82	0.22	0.17	—
HS-AlF$_3$	1.64	1.68	0.005	—
ACF + ^{15}N-pyridine	6.09	1.89	1.01	18
HS-AlF$_3$ + ^{15}N-pyridine	4.05	1.02	0.34	6

Table 5 Relative proportion of the acid sites of the samples as determined by simulation the ^{1}H MAS NMR spectra of ACF and *HS*-AlF$_3$ and the corresponding samples with adsorbed labelled pyridine

Sample	Brønsted	Lewis
ACF + ^{15}N-pyridine	1	3
HS-AlF$_3$ + ^{15}N-pyridine	1	2

was enough to generate these Brønsted acid sites on both solids. There is a remarkable difference in the intensity of the signals in the ^{1}H MAS NMR spectra of the ^{15}N-pyridine adsorbed sample of ACF compared with *HS*-AlF$_3$, see Fig. S1.‡ The adsorption of labeled pyridine was also confirmed by elemental analysis, as shown in Table 4. The data reveal that the amount of adsorbed pyridine onto the amorphous matrix of the mesoporous *HS*-AlF$_3$ is significantly lower than the adsorption onto ACF. These results agree with the lower intensity of the signals found in the ^{1}H MAS NMR spectra of pyridine-modified *HS*-AlF$_3$ with respect to those of ACF.

Under the conditions used for ^{1}H MAS NMR measurements with pyridine in which the nuclei are relaxed, distinction of protons belonging to the aromatic pyridine ring (binding coordinatively to Lewis acid sites) from those that interact with pyridine either *via* Brønsted acid sites is possible. Based on dmfit simulations of the experimental spectra (see below) an estimation of the Lewis and Brønsted acid centers becomes possible (see also ESI‡). The results of this simulation are gathered in Table 5, suggesting that there is a higher ratio of Lewis-to-Brønsted centers in ACF than in *HS*-AlF$_3$. However, the difference is small and is presumably within the errors of the integration of the NMR spectra and the dmfit simulation.

To confirm the presence of pyridinium in a different environment, ^{1}H–^{15}N CP-MAS NMR experiments with ^{15}N-pyridine adsorbed onto the surfaces of ACF and *HS*-AlF$_3$ were carried out. The spectrum for ACF in Fig. 9 shows two ^{15}N

signals at −178 ppm and −125.5 ppm, and in addition a shoulder at −138.7 ppm. The lowest frequency signal can be assigned to ^{15}N-pyridine molecules that bind to Brønsted acid sites, whereas the other two signals correspond to Lewis base/acid interactions of ^{15}N-pyridine at Lewis acidic centers. For *HS*-AlF$_3$, the ^{1}H–^{15}N CP-MAS NMR spectrum using the same experimental parameters as for the measurements with ACF shows only the signal of the Brønsted acid sites at −171 ppm; and the adjustment of the rotation frequency and contact time allowed us to resolve the spectrum, revealing finally the presence of an additional signal at −119.9 ppm that can be assigned to Lewis acid sites (Fig. 10). The ^{15}N chemical shifts are in a good agreement with previous reports dealing with pyridine and pyridinium adsorbed onto amorphous aluminum hydroxide fluoride.[11,48] Also, the overall chemical shift range is in good agreement compared to the observed chemical shift values of adsorbed pyridine and pyridinium on metal-substituted zeolites. The latter exhibit chemical shifts at −63.5 ppm and −169.5 ppm after transformation to the IUPAC CH$_3$NO$_2$ standard.[47]

The ^{1}H–^{15}N CP-MAS spectrum for pyridine on ACF has been simulated using the "dmift" software, and the results are illustrated on the right of Fig. 9.[49] In purple, the calculated contribution of the Brønsted acid sites (−178 ppm), and in green and turquoise the calculated contributions of the two Lewis sites (−125.5 ppm and −138.7 ppm, respectively) are depicted. The spectra of the two adsorbed pyridine molecules at Lewis acid sites show a distinct anisotropy. Overall, there is
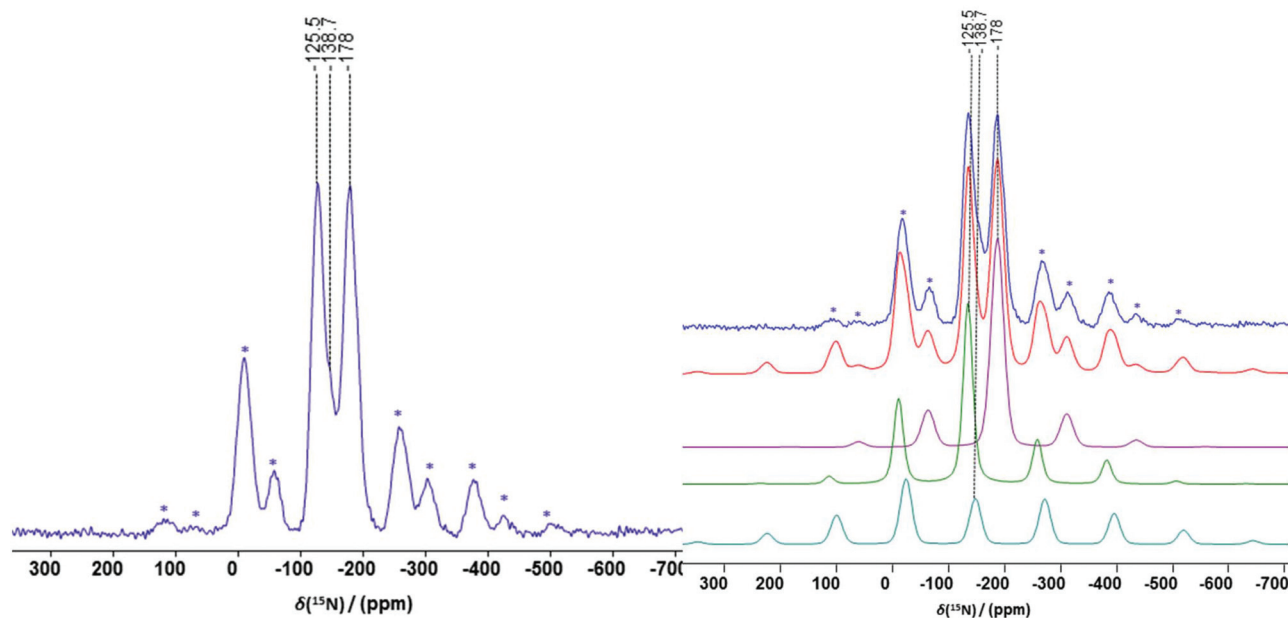
Fig. 9 Left spectrum: $^1H-^{15}N$ CP MAS spectrum of ACF treated with ^{15}N-pyridine. Asterisks (*) mark spinning sidebands; rotation frequency of 5 kHz. Right spectra: top blue trace corresponds to the measured $^1H-^{15}N$ CP MAS spectrum; subsequent traces are "dmfit" simulated spectra: in red the simulation of the full spectrum; in purple contribution of the Brønsted acid sites; in green and aqua contribution of Lewis acid sites. Asterisks (*) mark the prominent spinning sidebands (right).
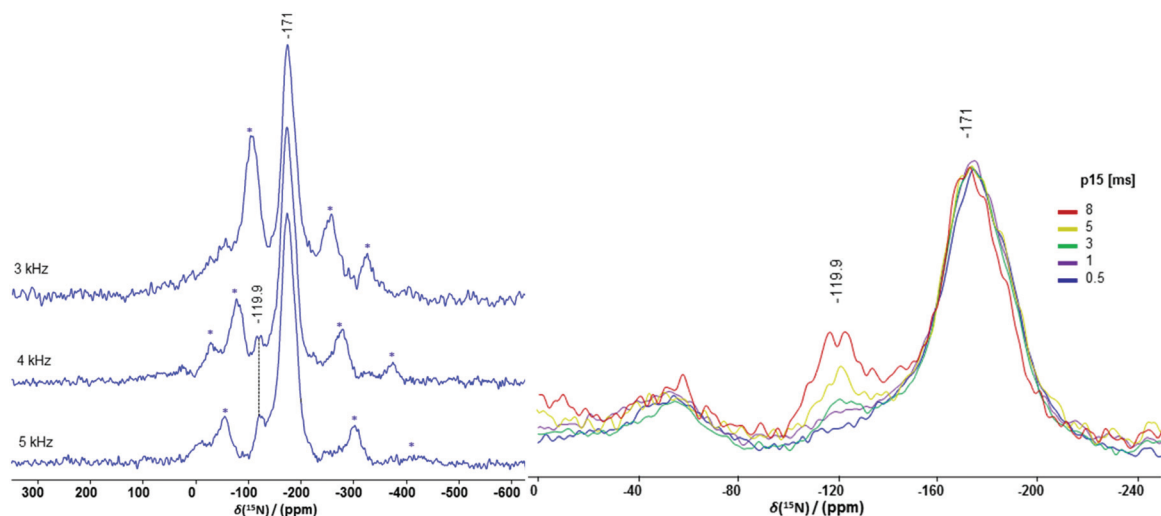
Fig. 10 Left spectra: $^1H-^{15}N$ CP MAS spectra of *HS*-AlF$_3$ treated with ^{15}N-pyridine at various rotation frequencies. Asterisks (*) mark spinning side-bands. Right spectra: $^1H-^{15}N$ CP MAS spectra of *HS*-AlF$_3$ treated with ^{15}N-pyridine applying different contact times, enlarging the area of the signals for the acidic centers; rotation frequency: 5 kHz.

a good agreement between the experimental and the simulated spectrum. With the simulation, the ratio between Lewis and Brønsted acid sites can be estimated as 3 : 1, thus resembling the ratio calculated from the integration of the ^1H MAS NMR spectra. Note that the quantification of the Lewis and Brønsted centers using "dmfit" simulation of the ^1H MAS and $^1H-^{15}N$ CP-MAS spectra should be regarded as a rough approximation. These results, however, confirm that ACF and *HS*-AlF$_3$ exhibit Lewis and Brønsted acid centers in their amorphous matrices

under the conditions employed here, although exclusively Lewis sites were expected. However, the extremely strong Lewis surface sites obviously take up water from the atmosphere under either experimental conditions thus forming Brønsted sites.

In Fig. 11, the ^{19}F NMR rotor-synchronized spin-echo MAS NMR spectra of pure ACF and *HS*-AlF$_3$ show the resonances corresponding to terminal fluorine atoms at about −202 ppm, which is in the case of high surface aluminum fluoride
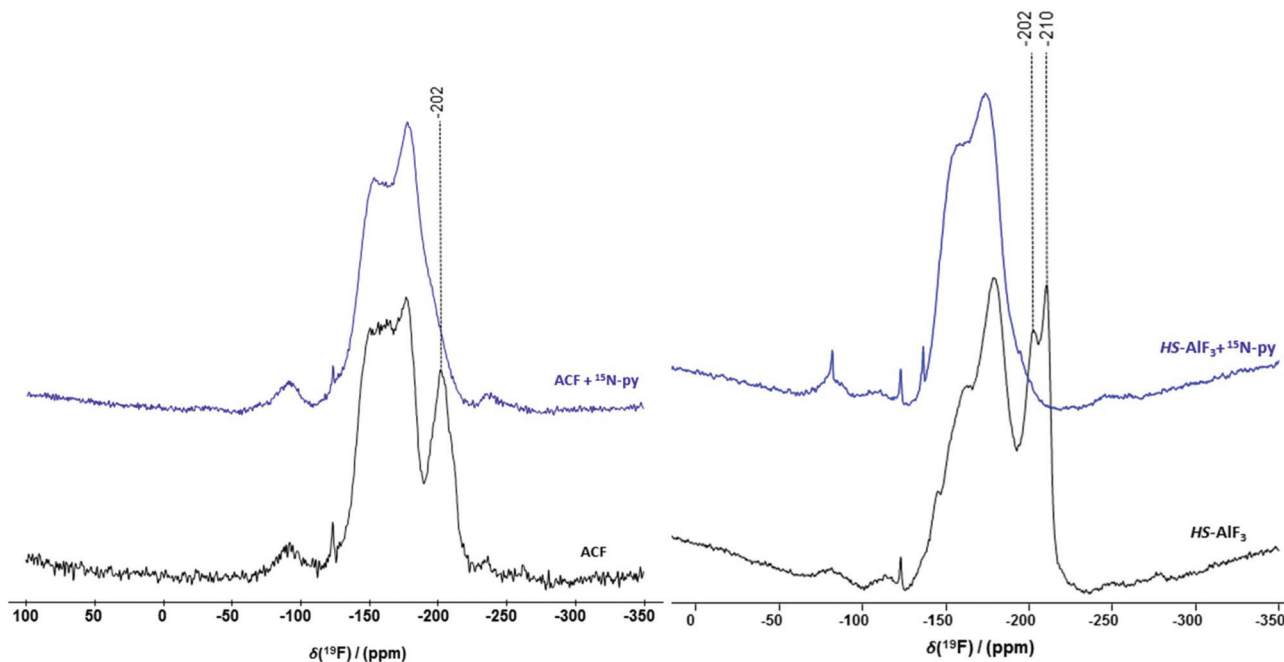
Fig. 11 ^{19}F MAS NMR rotor-synchronized spin-echo spectra of pure ACF (left, black) and *HS*-AlF$_3$ (right, black) and the samples after the treatment with ^{15}N-pyridine (blue). Rotation frequency: 20 kHz; dipolar evolution time: *t* = 0.25 ms, ns = 1024.

resolved as two peaks. These signals disappear upon the addition of pyridine (Fig. 11, spectra in blue), demonstrating that the terminal fluorine atoms undergo rearrangements when the solid materials accommodate the probe molecules at their surfaces. In view of the spectra in Fig. 11, it is most likely that the signals have shifted to higher frequencies forming part of the broad overlapping signals between −100 and −200 ppm.

Discussion

The comprehensive set of characteristic data for both, ACF and *HS*-AlF$_3$, obtained under exactly the same experimental conditions provides a deeper inside into not only the acidity of these catalysts, but also into their morphology. The sorption properties, which for these both AlF$_3$-phases differ, are not mainly due to differences in the surface acidity but obviously are strongly determined by topological differences. As shown by BET measurements, the pore size distribution differs remarkably between both catalysts, and consequently affects the observed surface acidity.

To explain the difference observed in their morphology, the synthesis procedure for each catalyst (see Introduction) needs to be considered. As said before, both phases are X-ray amorphous, which means indirectly that there is a high degree of structural distortion in them. In the case of ACF, such distortion is due to the alien chlorine atoms, whereas for *HS*-AlF$_3$ the distortion arises from the remaining isopropoxide groups inside the "as prepared *HS*-AlF$_3$", which in fact is an alu-

minium alkoxide fluoride, Al(OR)$_x$F$_{(3−x)}$ (*x* ≈ 0.7) (R = iPr). During the activation step with CHClF$_2$, these remaining organic groups in *HS*-AlF$_3$ presumably serve as a kind of space holder, thus creating larger pores in the mesoporous region in the course of OR$^−$ against fluoride exchange during the post fluorination process. ACF does not possess such groups, and so it will inevitably remain microporous.

The series of methods used in this work for characterizing the acid sites indicate altogether to a similar conclusion: the acid sites in ACF and *HS*-AlF$_3$ are in principle very similar, but the observed small differences arise from the different topological environment during the interaction of the probe molecule with the active sites of the pores. The accuracy of the acidity measurements is limited by the accessibility of active sites during the sorption of the probe molecule on the catalyst, and thus the morphological properties of the catalyst come to play an important role when comparing results.

In this work, carbon monoxide, pyridine, ammonia, and acetonitrile were used to probe surface acidity. As stated before, these molecules all have different size, polarizability (hard–soft base principle) and chemical binding properties. Thus, it is to expect that each of the characterization techniques presented here complements each other to give an overall picture of the acid sites in ACF and *HS*-AlF$_3$. Both catalysts exhibit a very similar distribution of acid sites showing different strengths. Differences in the amount of detected acidic sites with a certain Lewis acidity at the two catalysts with respect to each method, however, can be ascribed to their difference in porosity (CO) or the character of the probe molecule used (NH$_3$).

A contradiction arises from using pyridine as a probe molecule for MAS NMR spectroscopy studies, but can be easily explained. In the experimental set-up established here, the catalysts were suspended in labeled liquid pyridine for 1 h, and then dynamic vacuum (10^{-2} mbar) was applied for 17 h. Presumably, the easy adsorption/desorption of HS-AlF$_3$, and their bigger pores, allowed for more pyridine to be desorbed under vacuum than in the case of ACF. Thus, less pyridine seems to be adsorbed by HS-AlF$_3$, based on the MAS NMR spectroscopy analysis, but it is dependant on the kind of vacuum treatment that follows the adsorption step.

For CO adsorption, both phases exhibit similar IR bands at 2225 cm^{-1} and 2175 cm^{-1}, as an indication that the strength of the Lewis acid sites is likewise similar. Besides the position of the band, which determines the strength, the intensity also provides information about the relative amount of the acid sites. For similar CO pressures, HS-AlF$_3$ shows much more intense bands than ACF, since the former can better adsorb the probe molecule. This effect is also responsible for the difference in the ratio of the bands (very strong (2225 cm^{-1}) *vs.* strong (2175 cm^{-1}) sites) observed when comparing both phases at similar pressures. ACF seems to have relatively more very strong acid sites than HS-AlF$_3$, but mainly this appears because the experimental set up already generates a very high coverage of the sites in the mesoporous HS-AlF$_3$. Thus, the relative loading is too high for HS-AlF$_3$, and thus, a significant amount of the loaded CO becomes adsorbed already at the weaker, but still strong sites. Therefore, the lower ratio of very strong to strong Lewis acid sites observed for HS-AlF$_3$ under the experimental conditions employed here is rather due to different CO loadings for both solids than a real fact. This interpretation is supported by the results reported for FTIR-CO-adsorption measurements in the literature where lower partial pressures resulted in a very high ratio of very strong to strong Lewis acid sites (*cf.* insight of Fig. 5 right).[8] In other words, ACF and HS-AlF$_3$ show a different behaviour due to their sorption properties, but taking this into account, a comparison can still be made considering the experimental conditions (*i.e.* pressure range, since HS-AlF$_3$ sites are so rapid covered at low pressures, that very small steps need to be performed, whereas for ACF higher pressures are needed to exhibit adsorption of CO).

The intensities observed in CO adsorption bring to the discussion a main difference between ACF and HS-AlF$_3$: the former adsorbs almost five times less CO than the latter. This increased adsorption capacity is not easy to explain, since their surface areas (by BET) and number of acid sites (as determined by NH$_3$ TPD) are comparable. Ammonia is bound very strongly to the surface, whereas CO binds very weakly similarly as N$_2$ does. Considering gas-solid adsorption, ACF exhibits mainly micropores, as shown in Table 1 from the micropore volume obtained from the corresponding *t*-plot. The N$_2$ sorption isotherm depicts that even increasing the pressure does not enhance the quantity of N$_2$ adsorbed on ACF: 4 mmol of N$_2$ g^{-1} ACF are adsorbed, independent from the pressure. Likewise, desorption occurs without hindrance and no hyster-

esis is observed. On the other hand, HS-AlF$_3$ exhibits mostly mesopores, as seen from the low value of the micropore volume estimated. From the isotherm shape, more nitrogen is adsorbed than in the case of ACF, and at higher pressure (P/P^0 = 0.8) 15 mmol of N$_2$ g^{-1} HS-AlF$_3$ can be adsorbed: almost four times higher. The origin of these differences in adsorption arises from the synthesis procedure and will be discussed in more detail in following sections.

The ammonia TPD profiles of both phases are also alike, giving as well a similar amount of total acid sites, and the small differences appear in the shape of the desorption profile. Of course, because of the decomposition of ACF at around 400 °C, comparison of the desorption profiles of both phases has to be taken with care above 400 °C, but in general, it can be assumed that both catalysts possess comparable, very strong acid sites. In the medium temperature range, from 150 °C to 350 °C, the profile for ACF seems to be more structured and defined than the correspondent from HS-AlF$_3$. However, the observed higher NH$_3$-loading at weaker surface sites together with the mesoporosity in case of HS-AlF$_3$ will evidently alter the desorption behaviour when compared with the microporous ACF. A higher number of probe molecules is able to reach the acid sites in HS-AlF$_3$, and thus reach as well the weak acid sites, which for ACF are difficult to cover due to the small pore size. This interpretation is also in line with the other results, in which also the pore size seems to influence the final outcome.

Acetonitrile PAS-FTIR experiments also showed that both ACF and HS-AlF$_3$ possess very strong Lewis acid sites, the strongest ever reported by this characterization technique, an observation which helps to understand the outstanding catalytic activity observed for these solids for different reactions.[19] However, such very strong Lewis acid sites are able to interact even with traces of moisture to form Brønsted acid sites. Indication for Brønsted acid sites is not consistent with the expectation derived from the chemical composition of both solid phases, but since they exhibit extremely strong Lewis acid sites, uptake of moisture during sample preparation cannot be totally excluded. Thus, the Brønsted acid sites detected in the course of these investigations are most probably not formed during the synthesis but during sample preparation for the different techniques.

Conclusions

Aluminium chlorofluoride, ACF (AlCl$_x$F$_{3-x}$), and high surface aluminium fluoride, HS-AlF$_3$, are the strongest solid Lewis acids described so far. ACF, existing in a narrow chemical composition range of 0.3 > x > 0.1, can be considered in a rough approximation as an AlF$_3$-phase too. All well introduced spectroscopic techniques indicate comparable, extremely strong surface Lewis acid sites for both phases. Small but distinct differences in sorption behavior and catalytic reactions arise mainly from topological differences, ACF exhibits microporosity, whereas HS-AlF$_3$ is mesoporous.

In this study, both catalysts were systematically analyzed using a variety of probe molecules which could assess their very strong Lewis acid sites. A blue shift of 95 cm^{-1} for adsorbed CD_3CN was for the first time observed at an aluminium-based catalyst, ranking ACF and HS-AlF$_3$ as the strongest solid Lewis acids reported. The very strong acid sites of ACF were for the first time probed by CO adsorption followed by DRIFTS, resulting in the conclusion that they are similar to the ones already reported for HS-AlF$_3$. Each probe molecule, and each characterization method, provided altogether complementary information to better understand these exciting aluminium fluoride-based catalysts. This investigation brings about the advantages and limitations of surface characterization methods in studying these particular aluminium fluoride based systems.

Differences in the catalytic behavior are minor but mainly originate from the different nature of porosity. Catalytic reactions of larger molecules, as a rule, proceed faster with HS-AlF$_3$ as catalyst since it exhibits mesopores, whereas small molecules often are faster processed at ACF which exhibits microporosity. The high electron deficiency in line with the undercoordination of Al-surface sites enables these two AlF$_3$-phases to activate C–F as well as C–H bonds already at room temperature thus opening a wide field of catalytic reactions to be explored based on these two extremely strong solid Lewis acids.[22,23,27,50]

Conflicts of interest

There are no conflicts to declare.

Acknowledgements

References

1 A. Corma, *Chem. Rev.*, 1995, **95**, 559–614.

2 G. Ertl, H. Knözinger and J. Weitkamp, *Handbook of heterogeneous catalysis*, 1997.

3 S. Bordiga, C. Lamberti, F. Bonino, A. Travert and F. Thibault-Starzyk, *Chem. Soc. Rev.*, 2015, **44**, 7262–7341.

4 C. Lamberti, A. Zecchina, E. Groppo and S. Bordiga, *Chem. Soc. Rev.*, 2010, **39**, 4951.

5 G. Busca, *Catal. Today*, 1998, **41**, 191–206.

6 J. Ryczkowski, *Catal. Today*, 2001, **68**, 263–381.

7 C. Elschenbroich, *Organometallics*, John Wiley & Sons, Ltd, 2006.

8 C. Morterra and G. Magnacca, *Catal. Today*, 1996, **27**, 497–532.

9 N. S. Hush and M. L. Williams, *J. Mol. Spectrosc.*, 1974, **50**, 349–368.

10 K. Hadjiivanov and G. Vayssilov, *Adv. Catal.*, 2002, **47**, 307–511.

11 F. Hemmann, G. Scholz, K. Scheurell, E. Kemnitz and C. Jaeger, *J. Phys. Chem. C*, 2012, **116**, 10580–10585.

12 F. Hemmann, I. Agirrezabal-Telleria, C. Jaeger and E. Kemnitz, *RSC Adv.*, 2015, **5**, 89659–89668.

13 D. Michel, A. Germanus and H. Pfeifer, *J. Chem. Soc., Faraday Trans. 1*, 1982, **78**, 237.

14 A. A. Gurinov, Y. A. Rozhkova, A. Zukal, J. Čejka and I. G. Shenderovich, *Langmuir*, 2011, **27**, 12115–12123.

15 I. G. Shenderovich, G. Buntkowsky, A. Schreiber, E. Gedat, S. Sharif, J. Albrecht, N. S. Golubev, G. H. Findenegg and H.-H. Limbach, *J. Phys. Chem. B*, 2003, **107**, 11924–11939.

16 V. A. Petrov, C. G. Krespan and B. E. Smart, *J. Fluorine Chem.*, 1998, **89**, 125–130.

17 C. G. Krespan and D. A. Dixon, *J. Fluorine Chem.*, 1996, **77**, 117–126.

18 E. Kemnitz, U. Groß, S. Rüdiger and C. S. Shekar, *Angew. Chem., Int. Ed.*, 2003, **42**, 4251–4254.

19 T. Krahl and E. Kemnitz, *Catal. Sci. Technol.*, 2017, **7**, 773–796.

20 S. Rüdiger, G. Eltanany, U. Groß and E. Kemnitz, *J. Sol-Gel Sci. Technol.*, 2007, **41**, 299–311.

21 T. Krahl, *Amorphes Aluminiumchlorofluorid und -bromofluorid—die stärksten bekannten festen Lewis-Sauren*, 2005.

22 B. Calvo, J. Wuttke, T. Braun and E. Kemnitz, *ChemCatChem*, 2016, **8**, 1945–1950.

23 A. K. Siwek, M. Ahrens, M. Feist, T. Braun and E. Kemnitz, *ChemCatChem*, 2017, **9**, 839–845.

24 J. F. Kögel, D. A. Sorokin, A. Khvorost, M. Scott, K. Harms, D. Himmel, I. Krossing and J. Sundermeyer, *Chem. Sci.*, 2018, **9**, 245–253.

25 P. A. Morken and D. J. Burton, *J. Org. Chem.*, 1993, **58**, 1167–1172.

26 T. Krahl, A. Vimont, G. Eltanany, M. Daturi and E. Kemnitz, *J. Phys. Chem. C*, 2007, **111**, 18317–18325.

27 M. H. G. Prechtl, M. Teltewskoi, A. Dimitrov, E. Kemnitz and T. Braun, *Chem. – Eur. J.*, 2011, **17**, 14385–14388.

28 M. Ahrens, G. Scholz, T. Braun and E. Kemnitz, *Angew. Chem., Int. Ed.*, 2013, **52**, 5328–5332.

29 G. Meißner, D. Dirican, C. Jäger, T. Braun and E. Kemnitz, *Catal. Sci. Technol.*, 2017, **7**, 3348–3354.

30 C. G. Krespan, A. C. Sievert and F. J. Weigert, DuPont de Nemours, *US Pat.*, 5157171, CAN115:70904, 1992.

31 C. G. Krespan, DuPont de Nemours, *US Pat.*, 5162594, CAN117:69439, 1992.

32 W. D. Harkins and G. Jura, *J. Am. Chem. Soc.*, 1944, **66**, 1366–1373.

33 D. G. Cory and W. M. Ritchey, *J. Magn. Reson.*, 1988, **80**, 128–132.

34 T. Krahl and E. Kemnitz, *J. Fluorine Chem.*, 2006, **127**, 663–678.

35 B. C. Lippens, B. G. Linsen and J. H. d. Boer, *J. Catal.*, 1965, **4**, 319–323.

36 K. S. Rouquerol, J. Rouquerol, F. Llewellyn, P. Maurin and G. Sing, *Adsorption by Powders and Porous Solids: Principles, Methodology and Applications*, Elsevier Ltd., 2nd edn, 2014.

37 M. Thommes, K. Kaneko, A. V. Neimark, J. P. Olivier, F. Rodriguez-Reinoso, J. Rouquerol and K. S. W. Sing, *Pure Appl. Chem.*, 2015, **87**, 1051–1069.

38 T. Krahl, R. Stösser, E. Kemnitz, G. Scholz, M. Feist, G. Silly and J.-Y. Buzaré, *Inorg. Chem.*, 2003, **42**, 6474–6483.

39 E. A. Paukshtis and E. N. Yurchenko, *Russ. Chem. Rev.*, 1983, **52**, 242–258.

40 A. G. Pelmenschikov, R. A. van Santen, J. Jänchen and E. Meijer, *J. Phys. Chem.*, 1993, **97**, 11071–11074.

41 H. Knözinger and S. Huber, *J. Chem. Soc., Faraday Trans.*, 1998, **94**, 2047–2059.

42 W. Daniell, N. Y. Topsøe and H. Knözinger, *Langmuir*, 2001, **17**, 6233–6239.

43 E. Escalona Platero, M. Peñarroya Mentruit and C. Morterra, *Langmuir*, 1999, **15**, 5079–5087.

44 A. Vimont, J. C. Lavalley, A. Sahibed-Dine, C. Otero Arean, M. Rodríguez Delgado and M. Daturi, *J. Phys. Chem. B*, 2005, **109**, 9656–9664.

45 F. Thibault-Starzyk, A. Travert, J. Saussey and J. Lavalley, *Top. Catal.*, 1998, **6**, 111–118.

46 M. Tamura, K. Shimizu and A. Satsuma, *Appl. Catal., A*, 2012, **433–434**, 135–145.

47 W. R. Gunther, V. K. Michaelis, R. G. Griffin and Y. Roman-Leshkov, *J. Phys. Chem. C*, 2016, **120**, 28533–28544.

48 F. Hemmann, C. Jaeger and E. Kemnitz, *RSC Adv.*, 2014, **4**, 56900–56909.

49 D. Massiot, F. Fayon, M. Capron, I. King, S. Le Calvé, B. Alonso, J.-O. Durand, B. Bujoli, Z. Gan and G. Hoatson, *Magn. Reson. Chem.*, 2002, **40**, 70–76.

50 G. Meißner, K. Kretschmar, T. Braun and E. Kemnitz, *Angew. Chem., Int. Ed.*, 2017, **56**, 16338–16341.